Thermal, mechanical and fracture properties of reaction injection-moulded poly(urethane–urea)s

Anthony J. Ryan*, John L. Stanford and Richard H. Still
Polymer Science and Technology Group, Manchester Materials Science Centre, University of Manchester Institute of Science and Technology, PO Box 88, Manchester M60 1QD, UK
(Received 22 March 1990; revised 25 October 1990; accepted 30 October 1990)

A series of poly(urethane–urea)s similar to those used commercially (formed from a 4,4′-diphenylmethane diisocyanate-based polyisocyanate and a polyether triol in admixture with an aromatic diamine, 3,5-diethyltoluenediamine) were prepared, with appropriate catalysis over a wide range of composition, by reaction injection moulding (RIM). All reactants were thoroughly characterized prior to use and the polymers were formed on in-house RIM equipment under controlled processing conditions. The RIM materials formed ranged from translucent flexible elastomers to opaque rigid plastics depending on their composition and were characterized by dynamic mechanical thermal analysis (d.m.t.a.), tensile stress–strain and fracture mechanics studies. D.m.t.a. showed that (micro)phase separation had occurred during polymerization and the RIM materials had a non-equilibrium two-phase morphology. The modulus data from the tensile stress–strain studies were compared to the predictions of theories for two-phase materials. The comparative data showed good agreement, over a wide range of composition, to a model for materials comprising a co-continuous morphology. Fracture properties were determined using a single edge notch technique. Low hard-segment materials failed in a ductile manner accompanied by gross tearing, as observed on scanning electron microscopy fracture surfaces, with values of critical strain energy release rate, $G_{IC} > 6$ kJ m^{-2}. High hard-segment materials showed brittle failure with $G_{Ic} < 3$ kJ m^{-2}.

(Keywords: reaction injection moulding; poly(urethane–urea); 3,5-diethyltoluenediamine; morphology; dynamic mechanical thermal analysis; tensile stress–strain; fracture)

INTRODUCTION

Reaction injection moulding (RIM) is a method for the high-speed production of complex polymer parts directly from low-viscosity monomers or oligomers. The reactants are combined by high-pressure impingement mixing and then they fill a mould, under low pressure, where they complete reaction to give a polymer part. The formation of solid polymeric materials involves cross-linking or (micro)phase separation, or a combination of the two phenomena, and parts can often be demoulded in less than a minute. The fundamental science and engineering principles of RIM are described in a recent book by Macosko[1].

RIM materials are generally segmented block copolymers, the most common being polyurethane[2,3], poly(urethane–urea)s[4–6], polyureas[7–9] and poly(ether–amide)s[10,11]. The unique combination of physical properties available from segmented block copolymers is related to their (micro)phase separation. RIM polyurethanes, in particular, have been extensively investigated by Macosko and coworkers[1,3], and for linear model materials, the factors determining final properties are hard-segment content and crystallinity, the degree of (micro)phase separation and copolymer molar mass.

Similar model studies have been made by Willkomm and coworkers[8] on linear copolyureas based on 3,5-diethyltoluenediamine (DETDA), and these studies emphasize the improved physical and thermal properties of materials containing polyurea hard segments, compared with those of copolyurethanes. Such studies are in general agreement with published studies of poly(urethane–urea)s[1,4–6]. The improvement in poly(urethane–urea) and polyurea properties, compared with polyurethanes, occurs despite the hard segments being amorphous and arises due to the higher driving force to (micro)phase separation in the urea-containing systems. The present study focuses on non-linear poly(urethane–urea)s that are analogous to commercially available formulations such as Bayflex 110® (Bayer AG), Daltoflex® (ICI Plc) and Spectrim® (Dow Chemical USA).

The thermodynamics of diblock copolymer systems are complex[12,13] and beyond the scope of this article; however, a few major features will be highlighted. Owing to the competition between the enthalpy and entropy of (micro)mixing, like monomer units will begin to aggregate at some temperature to form equilibrium microstructures. This weak first-order process[12,13] is known as the order–disorder transition or the microphase-separation transition (MST), and the composition-dependent, equilibrium microstructures formed are predicted to be either a body-centred cubic array of spheres in a matrix or a two-dimensional, hexagonal array of rods in a matrix or alternating lamella. These structures have been observed experimentally by a number of workers[14,15].

* To whom correspondence should be addressed

0032-3861/91/081426-14

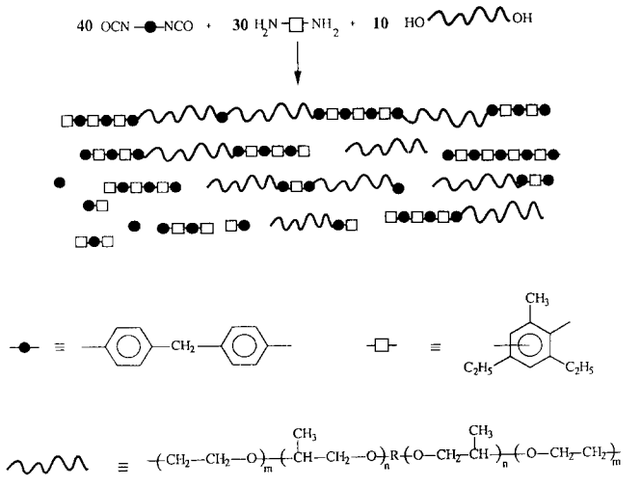

Scheme 1

The thermodynamics of segmented block copolymers are not at all well understood; theoretical predictions of the MST have been established[16] but predictions of morphology are not available at present. Experimentally, microstructures similar to those found for model diblocks have been observed by microscopy[17–19]. Generally, the polydispersity of segmented block copolymers means that imperfect microstructures form and bulk materials that pass from the bulk homogeneous (disordered) state through the MST into the ordered state are not at equilibrium; therefore, annealing has been observed to 'improve' morphology[19].

The formation of a linear poly(urethane–urea) (PUU) is shown in *Scheme 1*. Typically such a polymer could be formed from 4,4′-diphenylmethane diisocyanate (MDI) reacting with 3,5-diethyltoluene-diamine (DETDA) and a polyether diol (normally of molar mass 2000–4000). An alternating, segmented block copolymer is only formed in the special case of complete reaction[20]. At low conversions, the PUU-forming system is a mixture of monomers and short hard-segment sequences (the aromatic amine reacts ~10 times faster than the aliphatic alcohol[21] and catalysts that are preferential for the isocyanate–alcohol reaction are required). At higher conversions the material will be a mixture of unreacted polyether, short hard-segment sequences and di-, tri-, . . . , multiblock copolymers. The chemical reactions increase the degree of polymerization N and change the interaction parameter χ between the components. The increase in the product χN has been shown[22] to be equivalent to a thermodynamic quench from disordered or one-phase space into either the ordered (microphase-separated) region of the block copolymer microphase diagram or into the unstable region of the phase diagram of the mixture. Thus a multiblock copolymer will microphase-separate whereas a mixture of polymers or oligomers will macrophase-separate. The precise nature of the (micro)phase change in RIM materials is still unclear, i.e. micro- or macrophase separation.

In a previous paper[22] studies on phase separation in poly(urethane–urea)s and polyureas formed by RIM and the thermodynamics of segmented block copolymers were reviewed. The experimental data on RIM materials were interpreted in terms of the chemical reactions during RIM polymerization causing an enormous change in the thermodynamics of the system, which is analogous to a deep quench into the unstable region of the phase diagram. The existence of co-continuous morphologies, inferred from physical properties, was interpreted as a relic of spinodal decomposition where microphase separation was arrested before reaching equilibrium by vitrification of the hard-segment (micro)phase.

Phase separation in segmented copolyureas and poly(urethane–urea)s has also been studied[23] by investigating the formation of model polyurea–polyether blends with no covalent bonds between the phases. The polyblends have similar thermal and small-strain mechanical properties to the analogous copolymers (their moduli are identical from 50 to 200°C). Selective extraction of 80% of the polyether phase indicates its continuity. Scanning electron micrographs of internal fracture surfaces of the remaining hard-segment phase show a random continuous structure with a wavelength of ~200 nm. (This is an order of magnitude larger than the size scale observed by SAXS for RIM copolyureas by Willkomm *et al.*[8] and is due to the lack of interphase covalent bonding.) Thus this model polyurea–polyether blend has been shown to comprise a random co-continuous morphology, which has been interpreted as a relic of spinodal decomposition arrested by vitrification.

The thermal and mechanical properties of poly(urethane–urea)s have been investigated by a number of workers[4,5,7], but none gives a detailed description of the chemical system investigated nor reports studies over a wide range of composition. The interpretation of the dynamic mechanical spectra of RIM block copolymers is well established[2,3,5,6,8,10,11] but a detailed discussion of the stress–strain properties of RIM poly(urethane–urea)s is not available in the literature. There is also little information concerning the fracture properties of RIM materials. Shortall and coworkers[24,25] have studied the fracture properties of reinforced polyurethanes and Stanford has reported[26] studies of instrumented impact testing on reinforced polyurethanes. Papers from industrial laboratories often contain values of Izod impact strength for RIM poly(urethane–urea)s but these are generally from studies across limited composition ranges with poorly defined chemistry[5,7,27].

This paper reports systematic studies of the thermal, mechanical and fracture properties of a series of poly(urethane–urea)s, similar to those available commercially[1], but with well defined chemistry and processing conditions and over a range of composition. The results and discussion are presented under three headings, namely, dynamic mechanical thermal analysis, tensile stress–strain and fracture studies: where appropriate, the effects on properties of catalyst content and thermal history are also included. In contrast to previous studies of the fracture properties of RIM materials, attempts are made to determine fundamental materials fracture properties in terms of the critical strain energy release rate G_{Ic} and the critical stress intensity factor K_{Ic}, which are materials properties.

EXPERIMENTAL

Reactants

The materials in this study were formed using four components: (i) a polyisocyanate, (ii) a polyether polyol,

(iii) an aromatic diamine chain extender and (iv) an organometallic catalyst.

The polyisocyanate, Isonate RMA 400 (Dow Chemical), is a modified version of 4,4'-diphenylmethane diisocyanate (MDI) and is a straw-coloured, low-viscosity liquid (0.14 Pa s at 25°C) with a molar mass of 160 ± 2 g mol^{-1} by isocyanate titration[28].

The polyether polyol, Daltocel 32-75 (ICI Plc), is an oxypropylated derivative of glycerol, which has been further chain-extended with 15% by weight of oxyethylene and is nominally a triol with a relative molecular mass of 6000. It is a colourless liquid (0.53 Pa s at 35°C) with an equivalent weight of 1930 ± 30 g mol^{-1} (hydroxyl) by end-group analysis and a number-average molar mass of 5220 ± 80 g mol^{-1} by vapour-pressure osmometry[29].

The aromatic diamine, DETDA (Lonza AG), is nominally an 80:20 mixture of the 2,4 and 2,6 isomers of 3,5-diethyltoluenediamine. It is a brown liquid (0.07 Pa s at 35°C) that darkens on exposure to air. N.m.r. data confirm the isomeric nature of DETDA, and the as-received material had a purity of ~99% by gas–liquid chromatography[29].

The organometallic catalyst, T-12 (Air Products), is pure dibutyltin dilaurate (DBTDL) and had a tin content of 18.9% by weight (elemental analysis). All reactants were used as received without further purification.

Reaction injection moulding

Poly(urethane–urea)s were moulded as rectangular plaques (700 × 400 × 3 mm) using in-house RIM equipment that has been described in detail elsewhere[30]. The overall stoichiometric ratio, defined as the ratio of isocyanate to amine and hydroxyl groups, was held constant at 1.03. The catalyst concentration was held constant at 1.05×10^{-3} mol DBTDL per mole of isocyanate groups, except for the series of materials where the effect of catalyst content was studied. Hard-segment content, defined as the mass of DETDA plus the stoichiometric equivalent mass of isocyanate divided by the total mass of the system, was increased from 35 to 61% by increasing the ratio of DETDA to T32-75 in the polyol/diamine mixture. A constant machine throughput of 507 g s^{-1} was used for the polyol/diamine reactant stream and the corresponding throughputs of the polyisocyanate reactant stream were increased from 202 to 390 g s^{-1} to maintain reactant stoichiometry. Initial reactant and mould temperatures of 35 and 63°C, respectively, were used throughout, and typical gel times were of the order of 4 s, with mould filling occurring in less than 2 s. Plaques were removed from the mould after a period of at least 1 min. It is well established that, to achieve good mixing in an impingement mixing device, nozzle Reynolds numbers must exceed a critical value. Thus the polyol/diamine reactant stream Reynolds number was held constant at ~350, greater than the critical Reynolds number of ~300 generally quoted for poly(urethane–urea) formulations[1], whereas the polyisocyanate reactant stream Reynolds number was >1500. The materials were observed to be well mixed with no visible striations or gel lines. However, the higher hard-segment content materials were brittle and sometimes cracked in the mould.

Materials are designated using a code in which the capital letter refers to the diamine (D = DETDA), the number refers to the percentage hard-segment content and the lower-case letters refer to the thermal history (npc = as-moulded; pc = post-cured for 18 h at 100°C). Owing to the density difference between hard and soft segments, the volume fraction of aromatic material is within 1% of the hard-segment content calculated from stoichiometry, and thus hard-segment content and volume fraction are used interchangeably throughout.

Characterization of RIM materials

Post-cured (100°C/18 h) and as-moulded materials were characterized using dynamic mechanical thermal analysis (d.m.t.a.) and by tensile stress–strain measurements on dumb-bell specimens (ASTM D-638 M81) for Young's modulus, ultimate stress and ultimate strain and on notched strips for fracture mechanics analyses.

D.m.t.a. data were obtained on a Polymer Laboratories machine at a frequency of 1 Hz in the temperature range −100 to 300°C at a heating rate of 5°C min^{-1}. A double cantilever bending geometry was used for beam samples (3 × 10 × 45 mm) to obtain dynamic flexural moduli and mechanical damping as functions of temperature. Tensile stress–strain data were obtained on an Instron 1122 Universal Testing Machine at 20 ± 3°C. Dumb-bell specimens (ASTM D638m) having an overall length of 150 mm, a neck length of 60 mm, a width of 12.5 mm and a thickness of ~3 mm were used. The gauge length was 75 mm and the extension rate 10 mm min^{-1}. Strains were recorded to within ±0.05% using a 0–10% strain-gauge extensometer clamped directly on to the central portion of the dumb-bell specimen. The tensile properties reported are the mean of at least five tests.

Fracture mechanics measurements were made on an Instron 1122 Universal Testing Machine at 20 ± 3°C, at least 20 specimens being tested for each material. The single edge notch geometry used, for both K_c and G_c measurements, is illustrated in *Figure 1*. Notch depths a were varied from $0.05d$ to $0.6d$ with an extension rate of 10 mm min^{-1} and a gauge length l of 75 mm. The main depth of the notch was formed using a band saw and the last 0.5 mm of the notch was made using a fresh razor blade. In the case of G_c measurements the strain energy

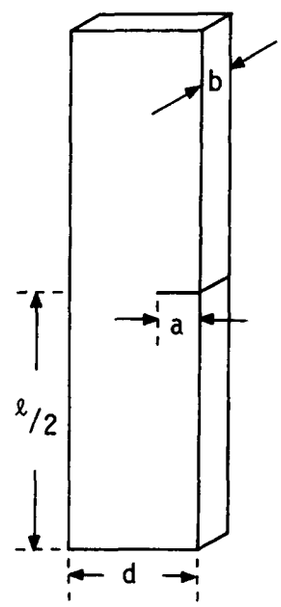

Figure 1 The single edge notch specimen geometry. Specimen dimensions are $1.2 \leqslant a \leqslant 15$ mm, $d \sim 25$ mm, $l \sim 130$ mm and $b \sim 3$ mm

density W_c in the specimen was determined from the integral of the stress–strain curve between zero deflection and the point of crack propagation as shown schematically in *Figure 2a*. For K_c measurements the elastic stress to fracture σ_c was determined from the stress–strain curves as shown in *Figure 2b*.

RESULTS AND DISCUSSION

The properties of poly(urethane–urea)s formed by RIM are dominated by their (micro)phase morphology comprising urethane end-linked, polyether soft segments and rigid, hydrogen-bonded polyurea hard segments. For these poly(urethane–urea)s, bulk copolymerization is equivalent to a thermodynamic quench from the monomers in one-phase space to a mixture of block copolymers and homopolymers in two-phase space, and recent experimental results indicate that spinodal decomposition may occur, forming materials with non-equilibrium, co-continuous morphologies[22,23]. During RIM processing it is essential to catalyse the hydroxyl–isocyanate reactions to avoid premature phase separation of the polyurea hard segments. The aromatic diamine reacts with the diisocyanate ~10 times faster than the uncatalysed polyether[21], and in order to produce microphase-separated materials with good interphase covalent bonding, the reactivities must be similar[5]. Thus the formation of poly(urethane–urea)s involves a competi-

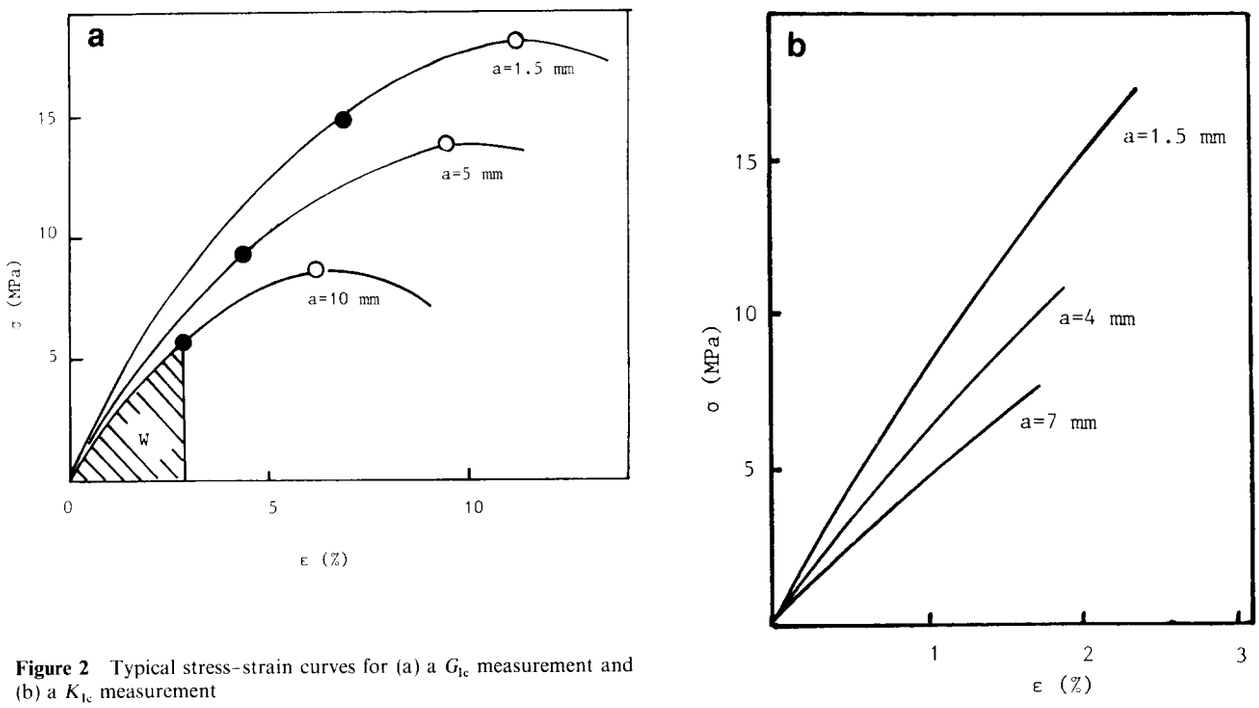

Figure 2 Typical stress–strain curves for (a) a G_{Ic} measurement and (b) a K_{Ic} measurement

Table 1 Dynamic mechanical thermal properties of RIM poly(urethane–urea)s

Material	T_g^S (°C)[a]	T_g^H (°C)[b]	$E'(-30°C)/E'(+65°C)$[c]	$E'(+65°C)/E'(+160°C)$[c]
D35pc	−51	185	3.7	2.1
D35npc	−50	177	4.4	2.2
D42pc	−47	183	4.2	2.0
D42npc	−45	179	3.9	2.1
D46pc	−46	190	2.9	1.9
D46npc	−46	190	3.3	2.0
D51(0.45[d])pc	−47	202	3.2	1.7
D51(1.05[d])pc	−46	194	3.5	1.8
D51(1.05[d])npc	−42	190	4.0	2.1
D51(1.35[d])pc	−44	184	3.6	1.9
D56pc	−45	195	3.2	2.0
D56npc	−43	195	3.0	1.8
D61pc	−48	196	2.8	1.8
D61npc	−48	193	2.9	1.8

[a] T_g^S = soft-segment glass transition temperature
[b] T_g^H = hard-segment glass transition temperature
[c] E' = dynamic flexural modulus
[d] Catalyst content × 10^3 mol DBTDL/mol NCO

tion between polymerization and (micro)phase separation, which may produce either a phase-separated mixture of polyurea and polyether with no interphase covalent bonds or a microphase-separated block copolymer network. In practice, materials with intermediate structures (complex mixtures of monomers, homopolymers and block copolymers) are formed, which are very difficult to describe within the framework of the Gibbs phase rule.

Dynamic mechanical thermal analysis

The dynamic mechanical properties of the poly(urethane–urea)s, derived from medial d.m.t.a. curves, are summarized in *Table 1*. The variation of flexural storage modulus E' with temperature for the post-cured poly(urethane–urea)s is shown in *Figure 3* and the corresponding tan δ curves are shown in *Figure 4*. Generally two major relaxations are observed, namely soft-segment and hard-segment glass transitions located at temperatures T_g^S (~ -48°C) and T_g^H (~ 175 to 205°C) respectively. A third, less intense, transition is observed between 50 and 100°C and is attributed to a mixed phase relaxation.

T_g^S is observed as a drop of approximately half a decade to a decade in the value of the storage modulus and as a corresponding peak in the tan δ and loss modulus curves. The value of T_g^S is relatively insensitive to the hard-segment content and is -48 ± 3°C. The intensity of the peak in tan δ associated with T_g^S changes in proportion to the weight fraction of polyether, and the peaks are broad, asymmetrical and do not return to the original baseline. A homogeneous polyurethane network made from T32-75 and MDI has a T_g of -52 ± 1°C, which compared to T_g^S indicates that there are some polyurea hard segments dissolved in the polyether phase of the poly(urethane–urea)s that raise and broaden this transition. Furthermore the asymmetric shapes of the peak suggest that there is some domain boundary mixing with an interfacial region having a shallow composition profile. This is fairly typical of segmented block copolymers, and Leung and Koberstein[31] have shown the mixed interphase to occupy up to 50% of the volume of model copolyurethanes.

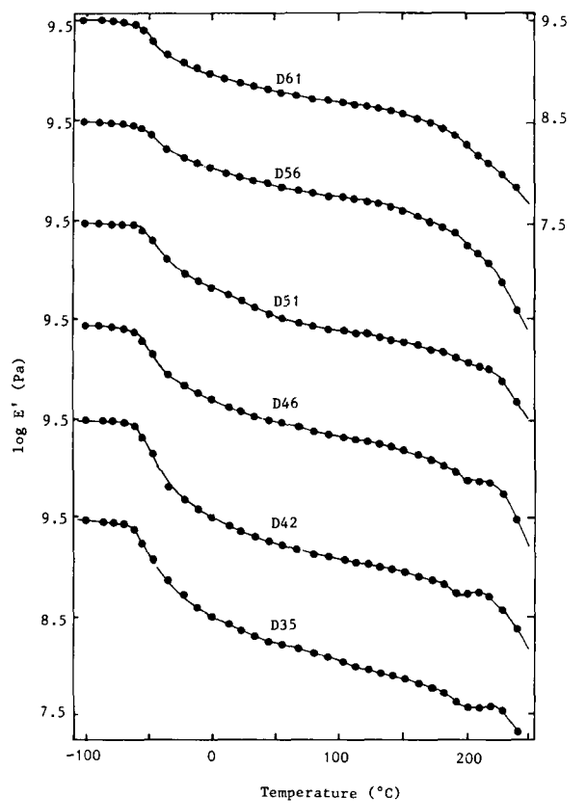

Figure 3 Flexural modulus E' *versus* temperature for the RIM poly(urethane–urea)s: curves have each been shifted by one decade for clarity

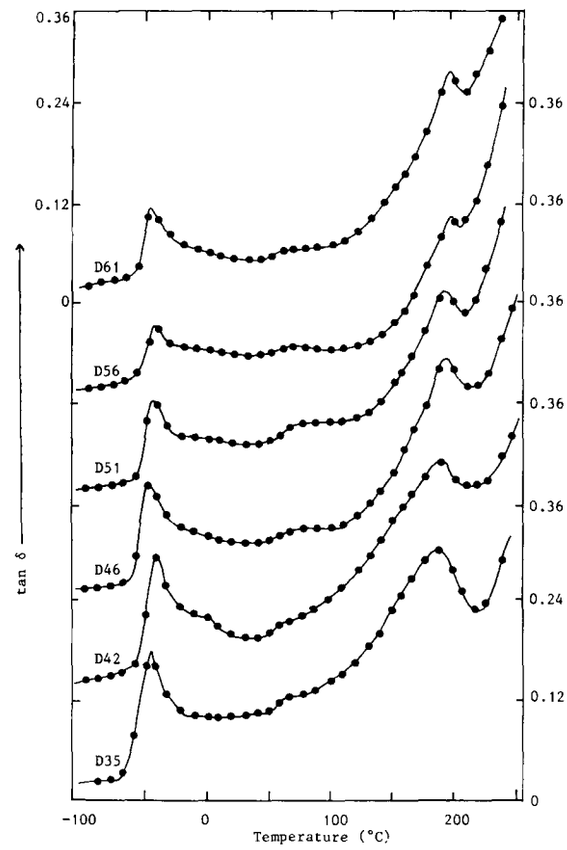

Figure 4 Mechanical damping, tan δ, *versus* temperature for the RIM poly(urethane–urea)s: curves have each been shifted by 0.12 for clarity

The value of T_g^H, however, is dependent on the hard-segment content and increases from 185 to 195°C as the hard-segment content increases from 35 to 65%. At low hard-segment content, T_g^H is observed as a definite peak in tan δ and a drop in modulus followed by a short rubbery plateau, whereas at high hard-segment content T_g^H is observed as a continuous decrease in modulus and as a shoulder superimposed on a rising tan δ curve. At high hard-segment content, T_g^H is swamped by large-scale, energy-absorbing molecular motions in a manner similar to that reported by Turner and coworkers[32] for similar polyurethanes. Dominguez and coworkers[27] have suggested that the catalysts for polymerization may also promote depolymerization and have reported the deleterious effects of added catalyst on the high-temperature properties of RIM polyureas. Thus it is possible that the T_g^H observed has been reduced by the plasticizing effects of low-molar-mass degradation products. In a previous paper[9] the T_g^H of a 35% hard-segment RIM polyurea (containing no catalyst) was reported to be 215°C, and this is higher than the value of $T_g^{H\infty}$ calculated for these poly(urethane–urea)s using the Flory–Fox equation[33].

In fact, it is higher than the T_g^H observed for D61. Willkomm and coworkers[8] have reported dynamic mechanical measurements on RIM polyureas, and while they observe a low-temperature peak clearly ascribed to T_g^S, low-intensity peaks, described as 'bumps', in tan δ observed around 200°C are not ascribed to T_g^H, but are explained in terms of degradation processes despite the reappearance of such peaks on cooling and reheating.

The shoulder in tan δ between 50 and 100°C is attributed to cooperative molecular relaxations of mixed soft and hard segments associated with intersegmental hydrogen-bond breakdown. Turner[4] labels a similar shoulder 'short-range ordering of hard segments' for similar RIM poly(urethane–urea)s, although an ordering process in an interphase with a composition gradient would be expected to be much broader than observed. Recent spectroscopic studies[34] of model polyurethane materials show evidence of urethane–ether hydrogen-bond lability in this temperature region, and intermediate shoulders on tan δ curves have been observed for a range of materials containing polyether and polyurethane or polyurea segments[4,5,9].

The temperature dependence of the modulus of RIM materials is often characterized by the ratio of moduli at the arbitrary temperatures of −30 and 65°C, these being the nominal limits of service temperature specified by the automotive industry[35]. The modulus ratio values $E'(-30°C)/E'(65°C)$ are given in *Table 1*, and the general trend is for the ratio to decrease with increasing hard segment, which reflects the value of E' at −30°C, a temperature that is close to T_g^S for these materials. Clearly, the ratio is very sensitive to the magnitude and rate of the modulus drop in the T_g^S region whereas the rate of change of modulus at 65°C is essentially constant. Although this ratio is often quoted it must be emphasized that the absolute value of modulus in this temperature interval is proportional to the hard-segment content and degree of (micro)phase separation. Camargo and coworkers[36] report modulus ratio values of 4 and 7 for catalysed and uncatalysed, linear RIM poly(urethane–urea)s based on DETDA/MDI/polyether diol, and these compare with the values of 3 and 4 observed in the present study for the catalysed, non-linear poly(urethane–urea)s.

The modulus temperature dependence at elevated temperatures is shown over an equal interval by the modulus ratio $E'(65°C)/E'(160°C)$, which when compared with the $E'(-30°C)/E'(65°C)$ ratios are not only lower but also show a much smaller dependence on hard-segment content. The $E'(65°C)/E'(160°C)$ ratios indicate the superior, prolonged, high-temperature dimensional stability of RIM poly(urethane–urea)s over RIM polyurethanes where the corresponding modulus ratios are an order of magnitude greater[2,3,30,32].

Comparison of the dynamic properties in *Table 1* shows that post-curing has a definite effect on materials properties. For example, the T_g^S of materials post-cured at 100°C for 18 h is -48 ± 3°C whereas T_g^S for as-moulded materials is -46 ± 4°C, and this may be interpreted as being due to an annealing effect, which allows greater phase separation, as the material moves closer to an equilibrium morphology, since at the post-curing temperature the mixed phase is molecularly mobile and its components may diffuse, against their concentration gradients (uphill diffusion), towards their respective phases. A similar shift in T_g^S was reported by Camargo[36]. Also, post-curing may allow free reactive

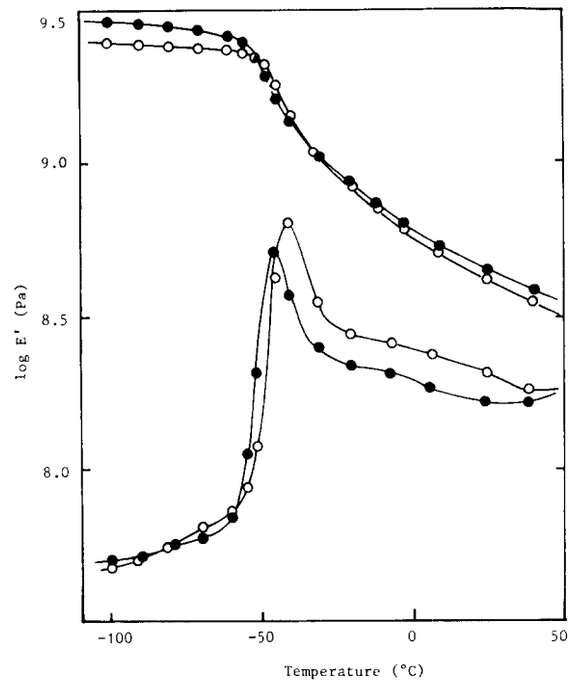

Figure 5 The effect of post-curing on the dynamic mechanical properties of RIM poly(urethane–urea)s: (○) D51(1.05)npc; (●) D51(1.05)pc

group encounters, thus increasing the interdomain covalent bonding and chemical crosslink density.

The effects of post-curing on the low-temperature modulus and damping behaviour of typical as-moulded and post-cured RIM poly(urethane–urea)s are shown in *Figure 5*. The location of the tan δ peak associated with T_g^S is shifted to a lower temperature, indicating a purer polyether phase. Furthermore, the level of damping is reduced by post-curing but the peaks do not sharpen significantly, indicating that both types of material have diffuse phase boundaries. Generally, the as-moulded materials have moduli lower than the post-cured materials, and this is due possibly to differences in chemical crosslink density.

Post-curing reduces the $E'(-30°C)/E'(65°C)$ ratio and this is due to the location of T_g^S; for example the T_g^S values for D51pc and D51npc are −46 and −42°C and the corresponding modulus ratios are 3.5 and 4.0. It may be readily observed from *Figure 5* that the rate of decrease of E' is far less for the post-cured material. Annealing improves phase separation and, intuitively, a perfectly microphase-separated block copolymer would have a modulus ratio of unity between the glass transitions when corrected for density changes. Post-curing has very little influence on the $E'(65°C)/E'(160°C)$ ratio, which remains at ~2. This temperature interval bounds the most stable region of the modulus plateau where the modulus is defined by the volume fraction of glassy polyurea material.

The effect of post-curing (18 h/100°C) on T_g^H is much less significant, as the annealing temperature is well below the transition temperature. Post-curing generally increases the values of T_g^H observed, although these data are in the limit of experimental error. A study of annealing close to the observed T_g^H was not possible due to blistering of the moulded material, due to the expansion of small gas bubbles and catalysed degradation of the hard

segments during post-cure, as observed previously by Nissen and Markovs[5].

A series of poly(urethane–urea)s were also made at a constant hard-segment content of 51% and catalyst concentrations of 0.45×10^{-3}, 1.05×10^{-3} and 1.35×10^{-3} mol DBTDL per mole of isocyanate group. The catalyst content had a profound effect on the moulding behaviour of the RIM poly(urethane–urea)s. The material with the lowest catalyst content shattered in the mould, the material with intermediate catalyst content cracked slightly on demoulding, whereas the material with the highest catalyst content could be removed from the mould intact. The differences in perceived toughness were less apparent after post-curing. Also, the material with the lowest catalyst content was opaque, whereas the other materials were translucent. This difference in light scattering indicates a difference in the size scale of (micro)phase separation.

The dynamic mechanical properties derived from medial d.m.t.a. curves of poly(urethane–urea)s made with different amounts of catalyst are summarized in *Table 1*. As catalyst content is increased, the value of T_g^S increases, and this may be observed in the low-temperature modulus and mechanical damping curves in *Figure 6*. Increasing catalyst content also has the effect of broadening the tan δ peak, and this may be interpreted in terms of the domain boundaries becoming more diffuse. The value of the modulus ratio $E'(-30°C)/E'(65°C)$ varies systematically with catalyst content, and this is consistent with the change in the glass transition. These observations are in good agreement with those of Camargo and coworkers[3] in which the modulus ratio for a model polyurethane decreased from 4.0 to 3.0 as the catalyst content was reduced from 0.75% to 0. In contrast to $E'(-30°C)/E'(65°C)$ the $E'(65°C)/E'(160°C)$ ratio is relatively insensitive to catalyst content as this property is dependent on the volume fraction of glassy polyurea material.

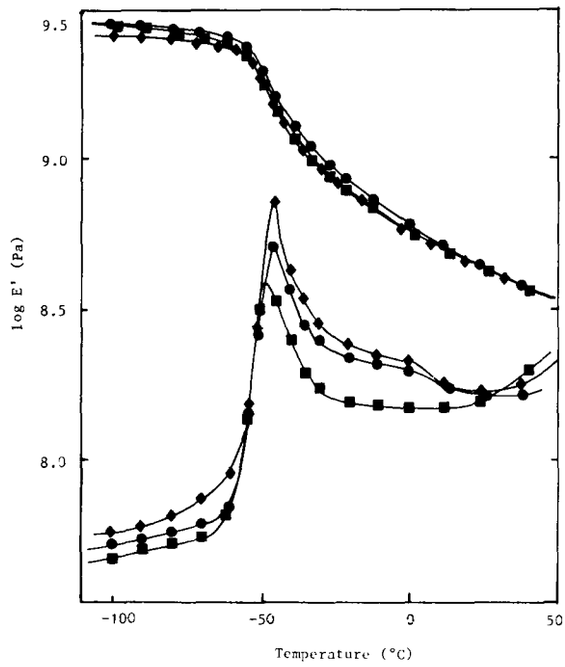

Figure 6 The effect of catalyst content on the dynamic mechanical properties of RIM poly(urethane–urea)s: (■) D51(0.45); (●) D51(1.05); (◆) D51(1.35)

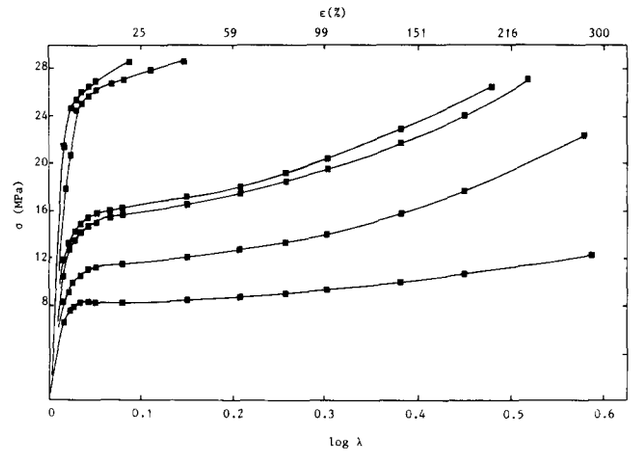

Figure 7 Representative stress–strain curves of RIM poly(urethane–urea)s. The uppermost curve is that of D61 and the lowest curve is that of D35

Increasing catalyst content reduces the value of observed T_g^H and this is most likely a combination of two effects. First, increasing catalyst content improves intersegmental covalent bonding and promotes microphase mixing. Secondly, this catalyst has been shown[7] to cause degradation in similar polyurea materials and hard-segment chain scission could produce low-molar-mass degradation products, which may bring about a reduction in the observed value of T_g^H.

The general effects of increasing catalyst content on the dynamic competition between polymerization and phase separation is to increase the rate of reaction (and the relative rate of hydroxyl to amine reaction) without affecting the characteristic time for (micro)phase separation. It is proposed that a low-catalyst-content material forms a mixture that (macro)phase-separates (until vitrification of the hard segments) with poor interphase covalent bonding, whereas a high-catalyst-content material forms a block copolymer that microphase-separates (until the hard-segment microphase vitrifies or chemical gelation occurs) with good interphase covalent bonding. For example, MDI reacting with DETDA in an unreactive polyether solvent (macro)phase-separates by spinodal decomposition to give a co-continuous morphology with a size scale of ~ 200 nm[23].

Tensile stress–strain studies

Tensile stress–strain curves for post-cured poly(urethane–urea)s are presented in *Figure 7* as stress *versus* log(extension ratio); this has the effect of expanding the initial portions of the curves relative to those based on stress *versus* engineering strain. The derived tensile properties are summarized in *Table 2*: values of modulus, ultimate stress and ultimate strain were first calculated from the force–deflection curves and then averaged, whereas the tensile toughness was derived directly from the averaged stress–strain curve.

The modulus and stress (at all strains) is increased with increasing hard-segment content due to the filler effect of increased glassy polyurea volume fraction. There is also an increase in physical crosslinking due to the hydrogen-bonded nature of the polyurea hard segments. There are two characteristic regions to the stress–strain curves. At low strains the materials have a high modulus and the slope of the stress–strain curve is very steep. All the materials show an extrinsic yield point that may be described using the Considere construction. The yield

Table 2 Tensile stress–strain properties of RIM poly(urethane–urea)s

Material	E^a (MPa)	$\sigma_u{}^b$ (MPa)	$\varepsilon_u{}^c$ (%)	$U_t{}^d$ (MJ m^{-3})
D35pc	258	12	320	48
D35npc	185	9	320	36
D42pc	322	23	287	70
D42npc	289	20	283	63
D46pc	423	27	228	68
D46npc	352	23	228	64
D51(0.45^e)pc	493	25	71	21
D51(1.05^e)pc	497	26	187	59
D51(1.05^e)npc	402	28	249	67
D51(1.35^e)pc	546	30	220	68
D56pc	689	28	37	15
D56npc	658	27	46	17
D61pc	735	28	17	6
D61npc	715	28	27	9

[a]Young's modulus
[b]Tensile strength
[c]Ultimate elongation
[d]Tensile toughness
[e]Catalyst content × 10^3 mol DBTDL/mol NCO

point is followed by extensive post-yield drawing with little increase in the nominal stress. Furthermore, two types of mechanical behaviour are evident from these tensile data. The lower hard-segment materials (D35 to D51) are semi-rigid elastomers with high values of tensile toughness and ultimate elongation, whereas the D56 and D61 materials have properties typical of a toughened, rigid plastic with higher moduli and lower ultimate elongations. This difference in mechanical behaviour is clearly demonstrated by the stress–strain data by pronounced changes in tensile properties at hard-segment contents between 51 and 56%, and this was originally reported[6,19,37] as being due to phase inversion from a polyether matrix with polyurea inclusions to a polyurea matrix with polyether inclusions. However, such interpretation is too simplistic for materials that clearly comprise complex morphologies, as shown by Bengtson and coworkers[38] for analogous solution-polymerized polyurethanes with stress–strain curves similar to those of the poly(urethane–urea)s. Such curves were interpreted as being typical of co-continuous (polycrystalline lamella) materials with the initial part of the curve arising from the deformation and yielding of the continuous hard-segment phase while the post-yield drawing is due principally to the deformation of the rubbery phase. Closer analysis of the stress–strain properties of the poly(urethane–urea)s is therefore required, particularly to differentiate between their low-strain (modulus) and high-strain (fracture) behaviour.

As indicated previously, the RIM materials are essentially composites in which the polyurea hard segments reinforce the polyether rubber or the polyether rubber toughens the polyurea glass. Several theories exist to predict the elastic properties of multiphase (composite) polymers and these, together with other properties, have been reviewed by Nielsen[39] and Dickie[40]. In the case of the present poly(urethane–urea)s, three theories have been used to model the low-strain, elastic behaviour in terms of predictive equations for composite moduli.

In the first, the upper and lower bounds of the modulus of a two-phase polymer material are given by the modified Kerner equation[41]:

$$G_c = G_1 \frac{\phi_1/v' + \phi_2 G_2/G'}{\phi_1/v' + \phi_2 G_1/G'} \qquad (1)$$

with $v' = 15(1 - v_1)$ and $G' = (7 - 5v_1)G_1 + (8 - 10v_1)G_2$, where G_c is the composite shear modulus, ϕ is the volume fraction ($1 = \phi_1 + \phi_2$), v_1 is Poisson's ratio, subscripts 1 and 2 refer to the matrix and the filler respectively and Kerner's theory requires the particles to be spherical in the mean.

In the second, for materials without well defined morphologies Budiansky[42] has developed a model that is a special case of the Kerner equation[41] (the packed grain limit). The model assumes that both components are continuous but the material is isotropic and macroscopically homogeneous. The composite modulus is obtained from a solution of the quadratic equation:

$$\phi_1(G_1 - G_c)(G_c + \alpha G_2) + \phi_2(G_2 - G_c)(G_c + \alpha G_1) = 0 \qquad (2)$$

where $\alpha = 2(5 - 4v_c)/(7 - 5v_c)$ and v_c is the Poisson's ratio of the composite and in this case is taken to be the weighted average of the Poisson's ratio of the two components.

In a third model, Davies[43] has used an expansion of the theoretical treatment of the dielectric constant of two-phase materials to develop an expression, with no adjustable parameters, to predict the shear modulus of materials with two interpenetrating continuous phases:

$$G_c^{1/5} = \phi_1 G_1^{1/5} + (1 - \phi_1)G_2^{1/5} \qquad (3)$$

According to Davies, the theory requires the existence of a perfect bond between the two phases, so that there is continuity of displacement across phase boundaries. (The theory rigorously demands that the bulk modulus of each phase should be infinite, i.e. incompressibility.)

Figure 8 is a semi-log plot of Young's modulus *versus* volume fraction of hard segment for the DETDA poly(urethane–urea)s. The upper and lower full curves

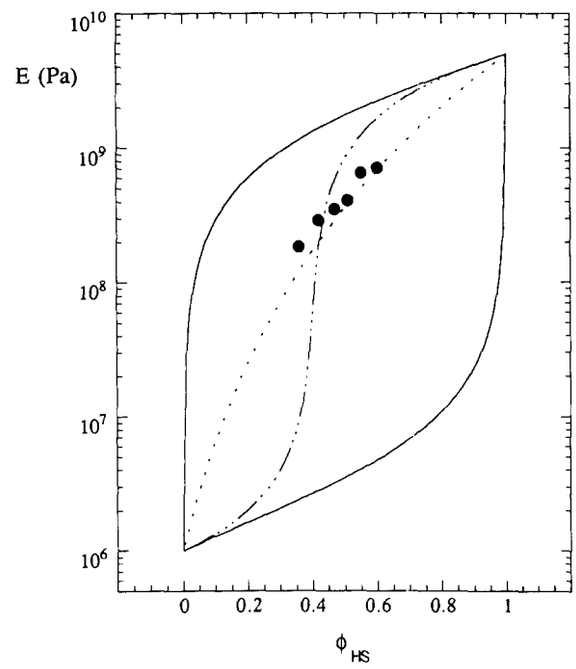

Figure 8 A semi-log plot of volume fraction of hard segment *versus* Young's modulus for DETDA-based poly(urethane–urea)s. The full circles are experimental data. The upper full curve is the prediction of the Kerner equation for a material with a glassy matrix; the dotted curve is the prediction of the Davies equation; the chain curve is the prediction of the Budiansky equation; and the lower full curve is the prediction of the Kerner equation for a material with a rubbery matrix

are the solutions to the Kerner equation for rubbery spheres in a glassy matrix and glassy spheres in a rubbery matrix, respectively. The dotted curve is the solution to the Davies equation and the chain curve is the solution to the Budiansky equation (Kerner packed grain) determined using the values of modulus and Poisson's ratio stated previously. The theoretical Young's moduli were calculated by substituting E for G in the equations and using values of the Young's modulus E of 1 MPa and a Poisson's ratio v of 0.5 for the polyether rubber[29] and values of 5 GPa for E and 0.35 for v for the polyurea glass[44]. In calculating the theoretical Young's modulus from Kerner's equation (1) and Budiansky's equation (2) for the theoretical shear modulus, the Poisson's ratio was weighted for composition. Davies' equation has the requirement that the bulk modulus be infinite, i.e. a Poisson's ratio of 0.5. The points are the measured values of the modulus for as-moulded RIM materials.

It may be readily observed from *Figure 8* that the present RIM materials give a good fit to the Davies equation for co-continuous materials and in the limit of composition studied do not conform to either bound of the Kerner equation for discontinuous–continuous morphologies, or correspond to the prediction of the Budiansky equation, which predicts phase inversion. The value of modulus is slightly higher than that predicted by the Davies equation because of the covalent bonds between the (micro)phases, which contribute to the material's stiffness. Allen *et al.*[45] have invoked the Davies equation to support the existence of well-bonded interpenetrating networks of polyurethane (PU) and poly(methyl methacrylate) (PMMA) over a wide range of composition. Furthermore good agreement with the modulus predicted by modifications of the Kerner equation were obtained for systems with PMMA spheres in a PU matrix. Klein *et al.*[46] have also used the Davies expression, which they class as a special solution to the Nielsen equation[39] for materials that are co-continuous. Using expressions for the shear modulus to calculate the Young's modulus does introduce some error, but this is small when compared to the predictions of the three different models and of the same order as the error in the measurement of Young's modulus.

The variations of modulus with copolymer composition for the DETDA-based poly(urethane–urea)s were originally interpreted[6,29,37] in terms of phase inversion occurring at $\phi \sim 0.5$. The step increase in modulus at 56% hard segment is relatively small and, as may be observed in *Figure 8*, the points are barely discernible from the co-continuous curve. However, the linear plot of modulus *versus* volume fraction, in *Figure 9a*, does infer some structural change in the materials. The existence of co-continuous phases does not preclude that the low hard-segment and high hard-segment materials have some morphological differences and this is borne out by the translucent appearance of D35 to D51 compared to the opacity of D56 and D61. The Davies equation makes no adjustment for the size of the phases or the interfacial area, which, of course, must change with hard-segment content. The likelihood of premature phase separation and thus coarser hard-segment phases and reduced interfacial covalent bonding is greater the higher the hard-segment content. However, the size scale of (micro)phase separation is observed to have little effect on modulus. For example, a blend of polyether/polyurea formed by RIM[23] having a co-continuous morphology

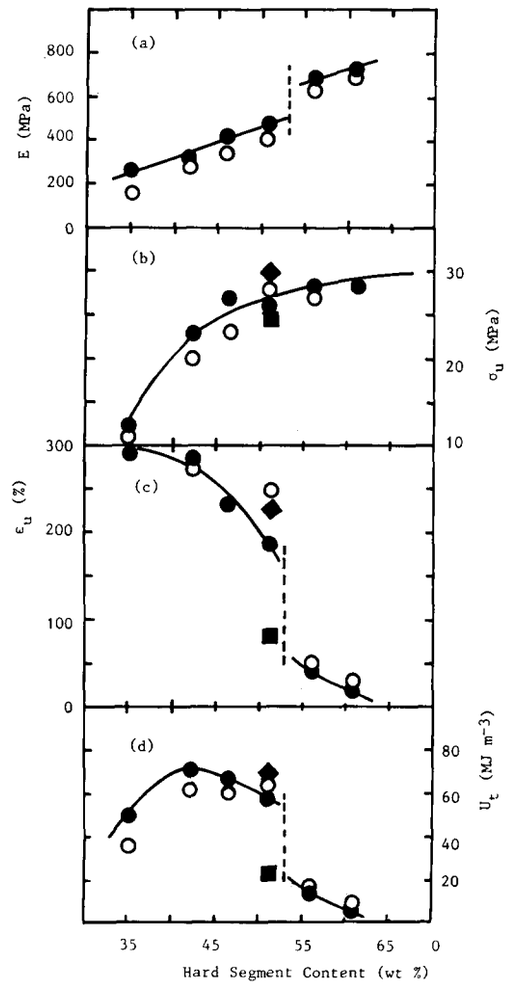

Figure 9 The effect of hard-segment content, catalyst content and post-curing on the tensile properties of RIM poly(urethane–urea)s: (a) Young's modulus E, (b) ultimate stress σ_u, (c) ultimate strain ε_u, and (d) tensile toughness U_t; (○) non-post-cured material; (●) post-cured material; (◆) D51(1.35); (■) D51(0.45)

with a size scale of ~200 nm has the same modulus, over a temperature interval of 150°C, as a RIM copolyurea[8] with a size scale of ~30 nm.

The ultimate stress (σ_u) *versus* volume fraction diagram (*Figure 9b*) shows an increase of σ_u with increasing hard-segment content up to a constant value of ~28 MPa. The ultimate properties of tensile test specimens are not materials properties in the same sense as the Young's modulus but a function of the specimen geometry and small imperfections in the samples. Thus the forms of the ultimate elongation (ε_u) and tensile toughness (U_t) curves (*Figures 9c* and *9d*) show step functions in properties around $\phi \sim 0.5$ and this was also previously interpreted[29] as an indication of phase inversion. For example, materials with hard-segment contents up to 51% have values of ε_u from ~200 to 300% whereas D56 and D61 have values of <40%. The corollary of this is the factor of 2 difference between the U_t values of D35 and D42, which arises from the difference in σ_u with both materials having similar elongations, or the factor of 3 difference in U_t between D51 and D56, which arises from the difference in ε_u with both materials having similar values of σ_u. The brittle nature of high hard-segment poly(urethane–urea)s and polyureas has been previously reported[5,7,8,27]. Dominguez and co-

workers[7,27] describe RIM materials that shattered prior to demoulding and had very low ultimate elongations. Willkomm and coworkers[8] discussed the contribution of free hard-segment oligomers to the brittleness of polyureas. Free hard-segment oligomers, which are expected to be more prevalent in poly(urethane–urea)s than in polyureas due to the lower reactivity of the soft-segment oligomer in the former, could also be the cause of the brittleness in the materials discussed here.

If the tensile properties of post-cured and as-moulded materials are compared (see *Table 2*), it may be observed that post-curing increases Young's modulus with no definite trend in the ultimate properties. The increased value of E may be ascribed to the increased phase connectivity brought about by post-curing, which overwhelms any annealing effects, as improved phase separation should lead to a reduced room-temperature modulus. Typical stress–strain curves for post-cured and as-moulded materials are shown in *Figure 10*. At all levels of strain, the stress is greater for the post-cured material and this is also a function of increased chemical crosslinking. At low hard-segment contents, the post-curing increases ε_u, and thus the dependent properties of σ_u and U_t show corresponding increases, which arise from the greater coherency of these materials. There is a much more complex relationship between the ultimate properties and thermal history for the higher hard-content materials.

The tensile stress–strain curves for post-cured D51 containing different amounts of catalyst are presented in *Figure 11* and the derived tensile properties are summarized in *Table 2*. The general effect of increasing catalyst content is to cause a small increase in modulus and increases in ε_u, σ_u and U_t. The increase in modulus is due to greater phase connectivity in the materials and accounts for the stress at all strains being higher for D51(1.35) compared with D51(1.05). The data for materials containing different amounts of catalyst have been included in the composition diagrams in *Figure 9*. The ε_u and U_t values of D51(0.45) lie close to those of D56 and D61 and the shape of the stress–strain curve is also similar. Furthermore, there were similarities between the moulding behaviour of D51(0.45), which was opaque and

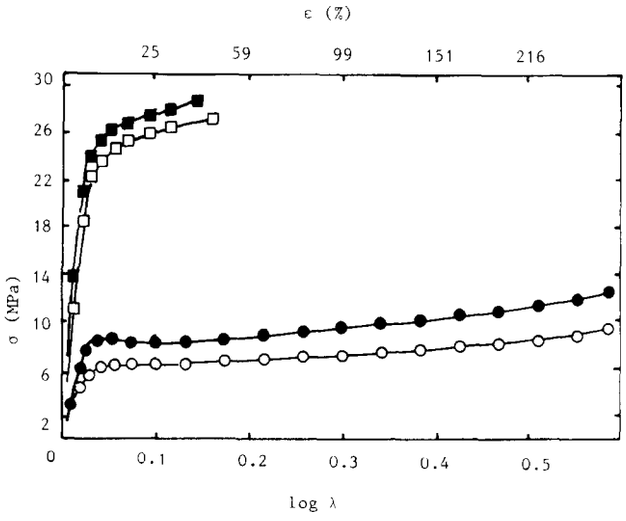

Figure 10 The effect of post-curing on the stress–strain curves of RIM poly(urethane–urea)s: (●) D35pc; (○) D35npc; (■) D56pc; (□) D56npc

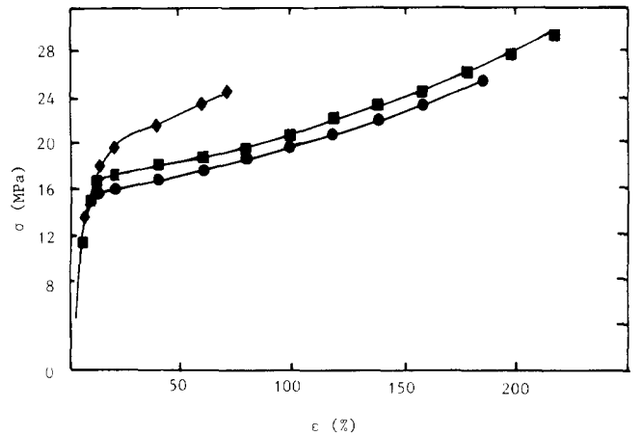

Figure 11 The effect of catalyst content on the tensile stress–strain curves of 51% hard-segment RIM poly(urethane–urea)s: (◆) D51(0.45); (●) D51(1.05); (■) D51(1.35)

cracked in the mould, and that of the higher hard-segment materials. Conversely, the materials with higher catalyst contents behaved in a similar manner to low hard-segment materials. As previously discussed, the relative reactivities of the amine and alcohol with isocyanate could lead to different types of material with different amounts of block copolymer character. The modulus is only sensitive to the co-continuity of the materials, with a lesser dependence on crosslink density, whereas the ultimate properties are sensitive to more subtle changes in morphology and molecular architecture.

Fracture mechanics studies

The RIM materials studied have a wide range of physical properties: at one extreme D61 has a modulus approaching 800 MPa and an ultimate elongation of 17% whereas D35 has a modulus of ~200 MPa and an ultimate elongation of >300%; and the tensile toughness of the materials, estimated from the area under the stress–strain curves, is 6 MJ m^{-3} for the former and 48 MJ m^{-3} for the latter. Therefore, to characterize the absolute fracture properties of this wide spectrum of materials using well established fracture tests is not trivial. The theoretical basis of the experiments to be discussed here is well established and has been reviewed in recent books[47,48] on the subject.

The low hard-segment materials may be treated as rubbers and their fracture behaviour analysed according to the tearing criteria of Rivlin and Thomas[49] to yield the tearing energy or more precisely the critical strain-energy release rate, G_{Ic}. The high hard-segment materials are brittle and their fracture behaviour is amenable to analysis using the theories of linear elastic fracture mechanics (LEFM)[47] to yield the fracture toughness, quantified by the critical stress intensity factor, K_{Ic}. More recently, slow restricted crack growth in ductile materials has been shown to give absolute fracture measurements by the J-integral approach[50]. However, the use of specimens with thick sections is necessary in order to fulfil the shape criteria for plane strain. However, the thickness of the RIM materials was limited to the thickness of the mould cavity, so that the geometry of these specimens was such that the criteria for plane-strain fracture conditions were not satisfied. In an attempt to overcome these problems and to make self-consistent

measurements of the fracture behaviour of RIM poly(urethane–urea)s, the single edge notch (SEN) technique was adopted using the tearing criterion to determine G_{Ic} values for the soft elastomeric RIM materials and the LEFM approach to determine K_{Ic} values for the stiff RIM materials.

During fracture testing of elastomeric materials, the instant of crack initiation is defined by Rivlin and Thomas[49] as the visible tearing associated with an increase in notch depth. The appropriate technique is to apply ink to the tip of the notch, and the point of crack initiation is determined as the first appearance of freshly torn un-inked material during a load–extension experiment. As reported in the 'Experimental' section, the load–extension curves were converted into stress–strain curves and the energy required to propagate the crack, W_c, was obtained by integrating the area up to the onset of crack propagation. The critical strain-energy release rate is defined, for this geometry, by the relation:

$$G_{Ic} = 2kW_c a \tag{4}$$

where a is the initial crack length; an approximate expression for k has been derived by Lake[51] as $k = \pi/\lambda_c^{1/2}$ where λ_c is the extension ratio of the specimen at the onset of crack propagation. Hence, G_{Ic} can be obtained from the slope of a plot of $2kW_c$ *versus* $1/a$, and a typical example of such a plot for the 42% hard-segment material is shown in *Figure 12*. Approximately 25 specimens are required to construct this figure and the reproducibility of the tearing analysis was established by using a separate plaque of D42 and a further 25 specimens to give a similar plot from which a second value of G_{Ic} was shown to be within 10% of the first value with a similar correlation coefficient. The $2kW_c$ *versus* $1/a$ plots were linear and passed through the origin and are therefore in good agreement with the predictions of fracture by tearing[49,52]. Owing to the nature of the fracture experiments it was very difficult to differentiate between as-moulded and post-cured materials. However, the similarity between fracture behaviour of as-moulded and post-cured materials may be due to long-term ageing (similar in effect to low-temperature annealing) of the former during the two-year period between moulding and fracture testing.

During testing of the more rigid materials, the instant of crack propagation corresponded to a rapid acceleration of the crack tip, and brittle fracture of the specimens resulted in force–deflection curves that were approximately triangular. The force required to propagate the cracks was obtained from the maxima in the curves, from

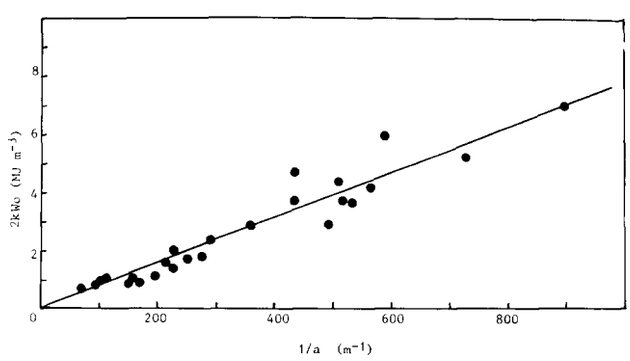

Figure 12 A typical critical strain-energy release rate determination: a plot of $2kW_0$ *versus* $1/a$ for D42

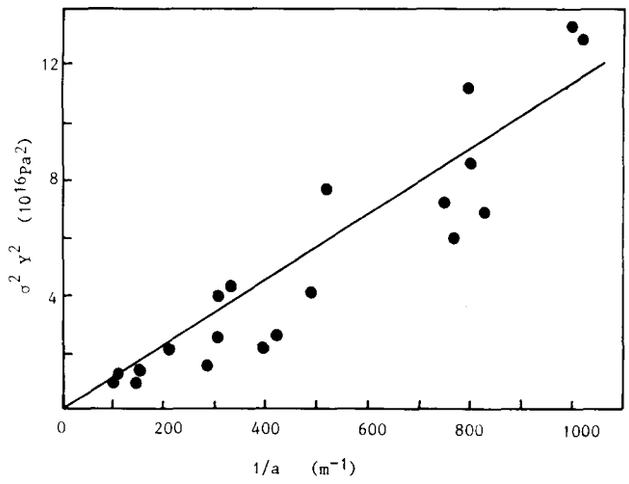

Figure 13 A typical critical stress intensity factor determination: plot of $\sigma_c^2 Y^2$ *versus* $1/a$ for D61

which the values of remote stress to failure, σ_c, were calculated. From the values of σ_c and the corresponding initial crack depths a, plots of $\sigma_c^2 Y^2$ *versus* $1/a$ were constructed according to:

$$K_{Ic}^2 = \sigma_c^2 Y^2 a \tag{5}$$

where Y is a shape factor for this specimen geometry[47]:

$$Y = 1.99 - 0.41(a/d) + 18.70(a/d)^2 - 38.48(a/d)^3 + 53.85(a/d)^4 \tag{6}$$

A typical example of such a plot is shown for D61 in *Figure 13*, and linear least-squares analysis gave the slope K_{Ic}^2 and a correlation coefficient of ~ 0.9. Similar analysis was performed for D51, and plots for both D51 and D61 were linear and passed through the origin, in good agreement with LEFM. The analysis for K_{Ic} is dependent on the specimens being under conditions of plane strain, that is, where the strain in one of the principal axes (the strain normal to the applied stress) is zero. According to Williams[47], the plane-strain criteria for SEN specimens of thickness b is:

$$b > 2.5(K_{Ic}/\sigma_y)^2 \tag{7}$$

where σ_y is the yield stress. D61 has an extrinsic yield stress of 25 MPa and the value of K_{Ic} determined from *Figure 13* is 1.08 MPa $m^{1/2}$. Thus for the plane-strain criteria to be fulfilled the specimen must have a thickness of $b \leqslant 4.7$ mm. The RIM mould had a constant thickness of 3 mm and therefore the values of K_{Ic} determined experimentally will be overestimated, as will the G_{Ic} values even though the latter have been calculated using the expression for plane stress:

$$G_{Ic} = K_{Ic}^2/E \tag{8}$$

Thus in *Table 3*, the values of K_{Ic} and G_{Ic} reported are not absolute, being intermediate to plane-stress and plane-strain behaviour. Nevertheless, they may be used in internal comparisons to show trends in materials properties. The data summarized in *Table 3* show that the value of G_{Ic} derived from SEN fracture measurements decreases with increasing hard-segment content. The values of U_t, obtained from the integrated area under the stress–strain curves show a similar downward trend. While there is a strong dependence of the crack

Table 3 Fracture properties of RIM poly(urethane–urea)

Material	G_{Ic} (kJ m^{-2})[a]	K_{Ic} (MPa m$^{1/2}$)[b]
D35	8.32	(1.47)
D42	7.72	(1.58)
D46	6.90	(1.71)
D51	3.12 (2.62)	1.14 (1.25)
D61	2.30 (1.59)	1.08 (1.30)

[a] G_{Ic} determined using the tearing analysis and urea under force–displacement curves; values in brackets calculated from measured K_{Ic} and E

[b] K_{Ic} values determined using the values of peak load and the corresponding notch depths; values in brackets calculated from measured G_{Ic} and E

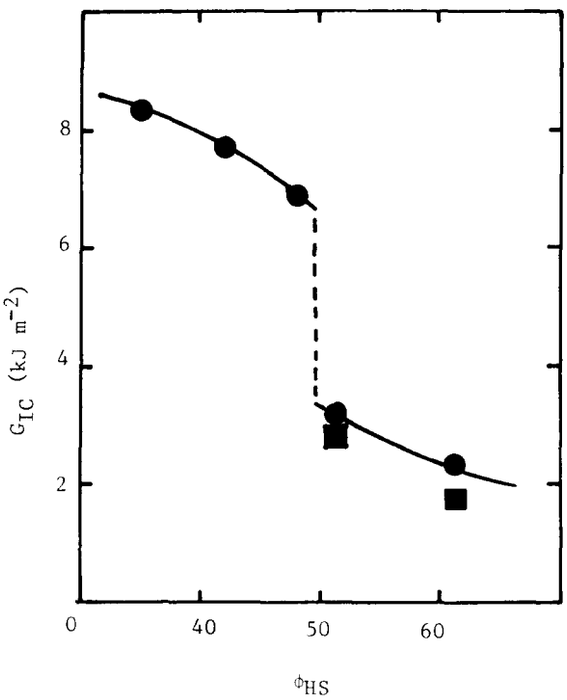

Figure 14 Plot of G_{Ic} *versus* composition for RIM poly(urethane–urea)s: (●) measured values of G_{Ic}; (■) values of G_{Ic} calculated from K_{Ic} and E

propagation energy G_{Ic} on hard-segment content, the resistance to crack initiation K_{Ic} is less sensitive to copolymer composition.

Figure 14 is a plot of fracture energy G_{Ic} *versus* hard-segment content for the post-cured poly(urethane–urea)s and shows a distinct transition in the fracture energy between 46 and 51% hard segment with G_{Ic} decreasing from 7 to 3 kJ m^{-2}. This transition is quite similar to the transition observed in the tensile properties–copolymer composition diagram in *Figure 9*. The two different types of behaviour depend on the dominant morphological structures. For example, D61 has a G_{Ic} of 1.59 kJ m^{-2} and this compares to the G_{Ic} values of 1.06 kJ m^{-2} quoted by Williams[47] for PMMA, and D61 has similar fracture behaviour similar to this classically brittle material. The value of G_{Ic} quoted by Kinloch and Young[48] for a rubber-toughened epoxy, a material comprising glassy and rubbery phases, is ~2 kJ m^{-2}, which is close to that of D61. However, the value of K_{Ic} for the epoxy is 2.2 MPa m$^{1/2}$, approximately double that of D61, and this is due to the much higher modulus of rubber-toughened epoxies. The fracture behaviour of the low hard-segment materials is more like that of classically tough materials such as medium-density polyethylene (MDPE), which has a G_{Ic} value of ~8 kJ m^{-2}, but much higher than the G_{Ic} values for natural rubber vulcanizates of 0.7 and 0.2 kJ m^{-2} reported by Rivlin and Thomas[49]. The fracture energy of a polyurethane network, based on MDI and a similar polyol to T32-75, was determined by the same technique to be ~0.5 kJ m^{-2} by Lee[53]. The low value of G_{Ic} is due to the friable nature of homogeneous poly(ether–urethane) networks. The poly(urethane–urea) materials discussed here comprise soft segments based on similar polyethers and the much higher G_{Ic} values obtained suggest a synergistic effect of incorporating a polyurea (micro)phase in the material.

Scanning electron micrographs of typical fracture surfaces are presented in *Figure 15* for D35, D51 and D61. The nature of the fracture process may be observed from the appearance of the fractured specimen. The surface of D35 shows gross tearing and there is also a

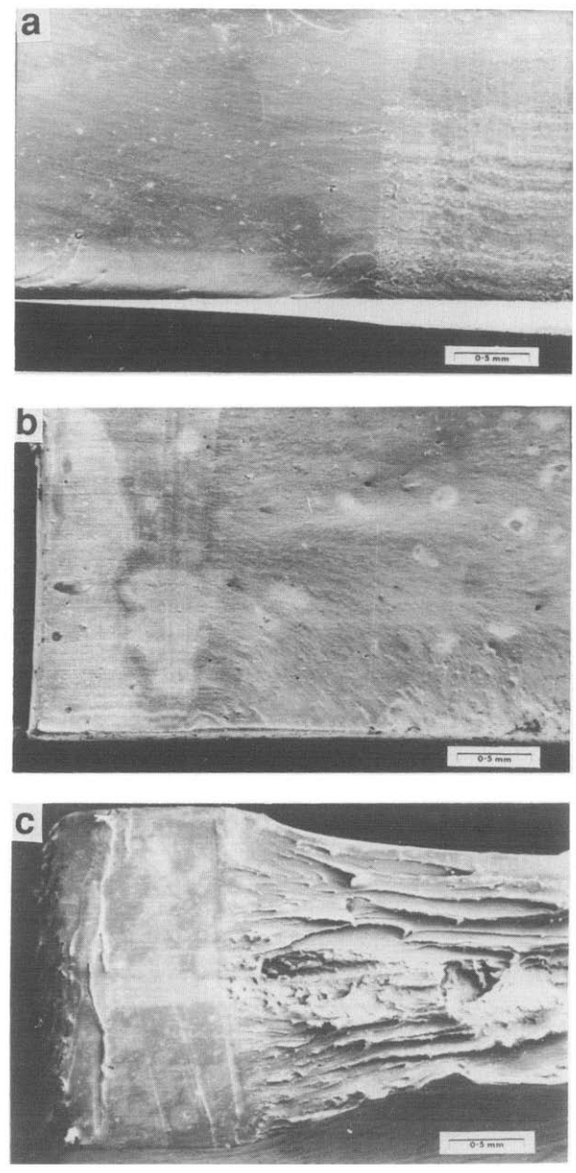

Figure 15 Comparative scanning electron micrographs of RIM poly(urethane–urea) fracture surfaces: (a) D61; (b) D51; (c) D35

significant reduction in the thickness of the specimen (from 3 to 2 mm) ahead of the notch. The reduction in cross section is due to local yielding resulting from stress concentration effects, and D35 has a yield stress of ~7 MPa. The fracture surfaces of D42 and D46 are very similar to D35, showing yielding and tearing, and these two materials have yield stresses of <15 MPa. All three materials were tested under conditions approximating to plane stress. In contrast, the micrographs of the stiffer and more brittle D51 and D61 specimens are smooth and almost featureless, showing very little surface damage other than that caused by the razor blade during notch formation. Also, because the yield stresses of these materials are much higher (17 and 25 MPa respectively), the specimens were tested under conditions approximating to plane strain and the specimen cross section does not show any reduction ahead of the notch.

SUMMARY AND CONCLUSIONS

The thermal, mechanical and fracture properties of a series of poly(urethane–urea)s have been determined as a function of composition over a wide range of hard-segment content, and the effects of varying catalyst content and thermal history have also been investigated. D.m.t.a. studies have shown (micro)phase separation to have occurred, and the annealing studies showed that the morphology, formed by (micro)phase separation competing with phase separation and copolymerization, was not an equilibrium morphology. Tensile stress–strain studies gave values of modulus that were in good agreement with those predicted by the Davies equation for co-continuous materials. The ultimate stress–strain properties, however, were very sensitive to composition, catalyst content and thermal history, and an apparent phase inversion occurred at $\phi \sim 0.5$, with the ultimate properties being dominated by the behaviour of the major (micro)phase. At $\phi \sim 0.5$, the material could be made to show both types of behaviour depending on catalyst content. The single edge notch fracture test was used for the full range of RIM materials. There was also a transition in fracture properties about $\phi \sim 0.5$, and the low hard-segment materials showed ductile fracture surfaces consistent with gross tearing and yielding, with $G_{Ic} > 6$ kJ m^{-2}. The high hard-segment materials showed brittle, featureless fracture surfaces and $G_{Ic} < 3$ kJ m^{-2}. However, the transition from ductile to brittle fracture was related to the yield stress of the materials and may have been an artifact due to specimen geometry.

These DETDA-based, RIM poly(urethane–urea)s, which are similar to those used commercially, have been studied over a wide range of composition and shown to have a co-continuous (micro)phase-separated morphology consistent with model studies[23] on analogous blends and linear block copolymers. This morphology has been shown to be a relic of spinodal decomposition arrested by vitrification and dominates the small-strain properties of the materials; the large-strain properties of these RIM materials were shown to be sensitive to copolymer composition, thermal history and, most importantly, catalyst content, which affects the relative rates of reaction and (micro)phase separation.

ACKNOWLEDGEMENTS

The authors would like to thank A. N. Wilkinson for helpful discussions. We would also wish to acknowledge D-K. Lee, who initially adapted the SEN technique for use in the characterization of the fracture properties of RIM materials.

REFERENCES

1 Macosko, C. W. 'RIM Fundamentals', Hanser, Munich, 1988
2 Camargo, R. E., Macosko, C. W., Tirrell, M. and Wellinghof, S. T. *Polym. Sci. Technol.* 1982, **18**, 95
3 Camargo, R. E., Macosko, C. W., Tirrell, M. and Wellinghof, S. T. *Polymer* 1985, **26**, 1145
4 Turner, R. B. *Polym. Compos.* 1984, **5**, 151
5 Nissen, D. and Markovs, R. A. *J. Elast. Plast.* 1983, **15**, 96
6 Ryan, A. J., Stanford, J. L. and Still, R. H. in 'Integration of Fundamental Polymer Science and Technology – 2' (Eds P. J. Lemstra and L. A. Kleintjens), Elsevier Applied Science, London, 1988
7 Dominguez, R. J. G. *J. Cell. Plast.* 1984, **20**, 433
8 Willkomm, W. R., Chen, Z. S., Macosko, C. W., Gobran, D. A. and Thomas, E. L. *Polym. Eng. Sci.* 1988, **28**, 888
9 Ryan, A. J., Stanford, J. L. and Wilkinson, A. N. *Polym. Bull.* 1987, **18**, 517
10 Gabbert, J. D. and Hedrick, R. M. *Polym. Proc. Eng.* 1986, **4**, 359
11 van der Loos, J. L. M. and van Geneen, A. A. *ACS Symp. Ser.* 1985, **270**, 181
12 Leibler, L. *Macromolecules* 1980, **13**, 1602
13 Frederickson, G. H. and Helfand, E. *J. Chem. Phys.* 1987, **87**, 697
14 See for example Folkes, M. J. and Keller, A. in 'The Physics of Glassy Polymers' (Ed. R. N. Haward), Wiley, New York, 1973, pp. 548–597
15 'Processing, Structure and Properties of Block Copolymers' (Ed. M. J. Folkes), Elsevier, New York, 1985
16 Benoit, H. and Hadziioannou, G. *Macromolecules* 1988, **21**, 1449
17 Chen-Tsai, C. H. Y., Thomas, E. L., MacKnight, W. J. and Schneider, N. S. *Polymer* 1986, **27**, 659
18 Li, C., Goodman, S. L., Albrecht, R. M. and Cooper, S. L. *Macromolecules* 1988, **21**, 2367
19 Goodman, S. L., Li, C., Cooper, S. L. and Albrecht, R. M. Proc. 46th Annu. Meet. Electron Microscopy Society of America, San Francisco Press, San Francisco, 1988, pp. 936–937
20 Peebles, L. H. Jr *Macromolecules* 1974, **7**, 872; 1976, **9**, 58
21 Pannone, M. C. and Macosko, C. W. *J. Appl. Polym. Sci.* 1987, **34**, 2409
22 Ryan, A. J., Stanford, J. L. and Still, R. H. *Plast. Rubber Proc. Appl.* 1990, **13**, 99
23 Ryan, A. J. *Polymer* 1990, **31**, 707
24 Dawson, J. R. and Shortall, J. B. *Cell. Polym.* 1982, **1**, 41
25 Parvisi, N. and Shortall, J. B. *Cell. Polym.* 1983, **2**, 251
26 Stanford, J. L. *AIChE Symp. Ser.* 1988, **260** (84), 74
27 Dominguez, R. J. G., Rice, D. M. and Grigsby, R. A. *Plast. Eng.* November 1987, p. 41
28 Stagg, H. E. *The Analyst* 1946, **71**, 557 (ASTM D1638M)
29 Ryan, A. J. PhD Thesis, Victoria University of Manchester, 1988
30 Barksby, N., Dunn, D., Kaye, A., Stanford, J. L. and Stepto, R. F. T. *ACS Symp. Ser.* 1985, **270**, 83
31 Leung, L. M. and Koberstein, J. T. *J. Polym. Sci., Polym. Phys. Edn* 1985, **23**, 1883
32 Turner, R. B., Spell, H. L. and Vanderhider, J. A. *Polym. Sci. Technol.* 1982, **18**, 63
33 Flory, P. J. and Fox, P. *J. Appl. Phys.* 1950, **21**, 581
34 Lee, H. S., Wang, Y. K. and Hsu, S. L. *Macromolecules* 1987, **20**, 2089
35 Ferrari, R. J. in 'Reaction Injection Moulding' (Ed. W. E. Becker), Van Nostrand Reinhold, New York, 1979, Ch. 4
36 Camargo, R. E., Andrews, J. S., Macosko, C. W. and Wellinghof, S. T. *Polym. Prepr.* 1984, **25** (2), 294
37 Ryan, A. J., Stanford, J. L. and Still, R. H. *Br. Polym. J.* 1988, **20**, 77
38 Bengtson, B., Feger, C., MacKnight, W. J. and Schneider, N. S. *Polymer* 1985, **26**, 895
39 Nielsen, L. E. 'Predicting the Properties of Mixtures', Dekker, New York, 1978
40 Dickie, R. A. in 'Polymer Blends' (Ed. D. R. Paul), Academic Press, New York, 1978, Ch. 8
41 Kerner, E. H. *Proc. Phys. Soc. Lond. (B)* 1956, **69**, 808
42 Budiansky, S. *J. Mech. Phys. Solids* 1965, **13**, 223
43 Davies, W. E. *J. Phys. (D) Appl. Phys.* 1971, **161**, 318, 1176, 1325

44 Katz, M. US Patent 288438, 1959 (*Chem. Abstr.* 1959, **53**, 17582b)
45 Allen, G., Bowden, M. J., Todd, S. M., Blendell, D. J., Jeffs, G. M. and Davies, W. E. A. *Polymer* 1974, **15**, 28
46 Klein, P. G., Ebdon, J. R. and Hourston, D. J. *Polymer* 1988, **29**, 1079
47 Williams, J. G. 'Fracture Mechanics of Polymers', Ellis Horwood, Chichester, 1984
48 Kinloch, A. J. and Young, R. J. 'Fracture Behaviour of Polymers', Applied Science, London, 1985
49 Rivlin, R. S. and Thomas, A. G. *J. Polym. Sci.* 1953, **10**, 291
50 Hashemi, S. and Williams, J. G. 'Deformation, Yield and Fracture', Conf. Proc. PRI, Cambridge, 1985, p. 53
51 Lake, G. J. 'Yield, Deformation and Fracture in Polymers', Conf. Proc. PRI, London, 1970, p. 531
52 Greensmiths, H. W. *J. Appl. Polym. Sci.* 1963, **7**, 993
53 Lee, D-K. PhD Thesis, Victoria University of Manchester, 1988